RSC Advances

ROYAL SOCIETY OF CHEMISTRY

www.rsc.org/advances

Graphical abstract

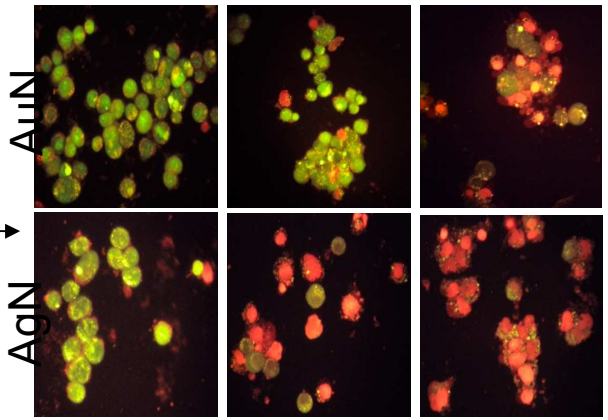

Morphological evidence of MCF-7 cell death

Biogenic metal (Ag and AuNPs)

Podophyllum hexandrum Royle

Green Synthesis

DNA damage

Bcl2/BaX regulation

Caspase Cascade

Mitochondrial dysfunction

Apoptosis

Molecular evidence of NPs induced apoptosis

RSC Advances

RSCPublishing

ARTICLE

Biogenic metal nanoformulations induce Bax/Bcl2 and caspase mediated mitochondrial dysfunction in human breast cancer cells (MCF 7)

Cite this: DOI: 10.1039/x0xx00000x

Received ooth January 2012,
Accepted ooth January 2012

DOI: 10.1039/x0xx00000x

www.rsc.org/

Murugaraj Jeyarai[a*$], Arun Renganathan[b$], Gnanasekar Sathishkumar[c], Andy Ganapathi[c], Kumpati Premkumar[d]

Nanostructures of noble metals were extensively studied in the recent past because of their stupendous physiochemical properties and wide range of applications in biology and medicine. In this study, anticancer efficacy of green synthesized metal nanoparticles (Ag & AuNPs) was assessed against human breast carcinoma cells (MCF-7). Treatment with different concentrations of NPs triggers the cellular toxicity in dose and time dependent manner. Morphological features of apoptosis were measured through cell wall integrity, Acridine orange/ Ethidium bromide and Hochest staining methods which clearly distinguishes the viable cells and cells undergoing apoptosis. Flow cytometer and DNA fragmentation analysis were also substantiate that NPs induced cytotoxicity was primarily mediated by G2/M cell cycle arrest and apoptosis. NPs provoke intracellular reactive oxygen species that causes damage to various cellular components. Moreover, the gene expression studies such as RT-PCR, qpCR and western blot analysis shows the up regulation of Bax, BCl2, caspases -6 & 9, PARP, p53 and down regulation of Bcl-2 depicts the induction of apoptosis upon NPs exposure. The overall results clearly denotes that green synthesized metal NPs can potentially inhibit the proliferation of MCF-7 cells and trigger apoptosis through Bax/Bcl2 and caspase-cascade mediated mitochondrial dysfunction. It concludes that biogenic metal nano-drug formulation can be utilized for cancer chemotherapy.

1. Introduction

In earlier reports, biological synthesis and assembly of metal nanoparticles have been discussed elaborately. Now it's very important to extend this active nanomaterial research towards drug development for various deadliest diseases like cancer, malaria, AIDS and tuberculosis. Among them cancer has always been one of the most potent scourges of mankind, that causes six million deaths and more than ten million new cancer cases every year worldwide (WHO). It was also mentioned that by the end of 2020 incidence of newer cancer cases will encounter two fold increases.[1] In particular breast cancer is the most common malignancy among women in the most developed and developing regions of world accounting for 23% of all female cancers. Incidence rates of breast cancer varied between countries with respect to age, social economic background, geographic distribution, stage at presentation and biological characteristics.[2]

Eventually, many cancer patients in worldwide were receiving some forms of chemotherapy in the hope of prolonging their life. However, two major limitations of traditional chemotherapy are dose-limiting systemic toxicity, which induce toxic responses in rapidly dividing cells and prevalence of multiple drug resistance (MDR).[3] To conquer this situation there is an urgent need of new tools and technologies with more specificity, cost effective and limited side effects to improve the quality of cancer patients life.

Nanotechnology based combinational therapy offers an extremely effective contrivance for cancer treatment which limits the detrimental side effects and prevalence of multiple drug resistance (MDR).[4] There are different types of nanoformulations such as liposomes, dendrimers, polymeric micelle, carbon nanotubes and magnetic nanoparticles have

been successfully developed towards early diagnosis and treatment of cancer.[5] Among the other nanomaterials metallic nanoparticles especially, noble metals like silver and gold nanoparticles emerged with the highest degree of commercialization and extensive biomedical applications.

On the other hand, combination of nanotechnology and molecular biology provides a new paradigm for cancer treatment through the identification of novel molecular targets at various stages of carcinogenesis. Especially, apoptosis remain to be a key denominator for many of these approaches in the elimination of cancer cells. Central to the execution of apoptosis is mediated by a class of cysteine proteases called caspases that has been activated either through death receptor activation or mitochondrial membrane permeabilization.[6] Several other protein families such as Bcl-2 and Bax were also influences the regulation of programmed cell death, hence the up and down regulation these proteins ultimately determine the cell death.[7-8]

The cytotoxicity effects of inorganic NPs were strongly influenced by their size, shape, surface chemistry and ability to bind with biological macromolecules.[9-11] Studies on different cell lines proved that metal NPs can easily cross through the cellular barriers and cause DNA damage, chromosomal aberrations and finally cell cycle arrest.[12] Biological synthesis of metal nanoparticles using pharmacologically important plant entities have been shown enhanced biological activities due to their surface functionalization with bioactive metabolites. In this study we have investigated the molecular mechanism involved in biogenic metal NPs induced cytotoxicity against human breast carcinoma cells (MCF-7).

2. Experimental Section

2.1. Materials

Silver nitrate ($AgNO_3$), Chloroauric acid ($HAuCl_4$), cisplatin, Hoechst 33258, 3-(4,5-dimethyl- 2-thiazolyl)-2,5-diphenyl-2H-tetrazolium bromide (MTT), 2-7-diacetyl dichlorofluorescein (DCFH-DH), heat inactivated fetal calf serum (FBS), minimum essential medium (MEM), glutamine, EDTA and trypsin were purchased from Sigma–Aldrich (St. Louis, USA). Breast cancer cell line (MCF-7) was obtained from National Centre for Cell Science (NCCS), Pune, India. The MCF-7 cells were grown as monolayer in MEM, supplemented with 10% FBS, 1% glutamine, and 100 U/ml Penicillin - Streptomycin and incubated at 37^{o}C in 5% CO_2 atmosphere. Stocks were maintained in 75 cm^2 tissue culture flask.

2.2. Synthesis and characterization of biogenic AgNPs

Podophyllum hexandrum Royle leaf extract was employed as reducing and stabilizing bioagent for the synthesis of Ag & AuNPs. Physiochemical properties of synthesized NPs were characterized through UV−Vis spectrophotometer, Transmission Electron Microscope (TEM), X-Ray Diffractometer (XRD) and Fourier Transform Infrared Spectroscopy (FTIR) as per our earlier reports.[13-14]

2.3. Invitro anticancer effect of biogenic NPs

2.3.1 Cytotoxicity Assay

The cytotoxicity of NPs were measured in MTT (3-(4, 5-dimethylthiazol-2-yl)-2, 5- diphenyl tetrazolium bromide) assay as described earlier.[15] Briefly, cells were seeded at a density of $5X10^4$ cells/well per 96-well plates. After 24 h, the cells were treated with NPs at various concentrations (50–250µl/ml) and incubated for 24h. At the end of the incubation, 10 µl of MTT (5 mg/ml) per well was added and incubated in dark at 37°C for 4 h. The formazan crystals formed after 4 h were solubilized in 100 µl of DMSO after aspirating the medium. The absorbance was monitored at 570 nm (measurement) and 630 nm (reference) using a 96-well plate reader (Bio-Rad, Hercules, CA, USA). Each growth curve showed the means and standard deviation (SD) of at least three independent experiments. The growth inhibition was determined using: growth inhibition = (control O.D.-sample O.D.)/control O.D. The IC50 value was defined as the concentration of NPs that produced a 50% reduction of cell viability.

2.3.2 Cytomorphological evaluation by phase contrast microscopy

After the incubation with NPs at their mentioned concentrations for 24h the gross morphological changes in the cells were observed under an inverted phase contrast microscope (Nikon, Japan) and photographed using a Nikon Digital camera (Nikon, Japan).

Evaluation of apoptosis

2.3.3. Acridine orange (AO) and Ethidium Bromide (EB) staining

The extent of apoptosis induced by NPs was identified by the morphological changes in MCF-7 cells after 24 h of incubation.[16] Cells were harvested and suspended in phosphate buffered saline solution (PBS). Cells were stained with 5 µl of cocktail mix containing AO (100 µg/ml) and EB (100 µg/ml) in PBS. A cell suspension of 10 µl was applied to a glass slide, covered with a cover slip and cells were viewed and photographed under a fluorescent microscope (Nikon 80i Eclipse, Japan). Viable cells are identified by a bright green nucleus with intact structure. Early apoptotic cells show bright green nucleus with condensed chromatin, while nuclei of apoptotic cells in the late phase stained with orange and shows condensed chromatin structure. Whereas necrotic cells displays orange nucleus without condensed chromatin. At least 200 cells were counted for each condition tested.

2.3.4. Hoechst 33258 staining

The nuclear changes and apoptotic bodies induced by NPs were characterized by Hoechst 33258 staining. Briefly, cells in the 24-well plates were trypsinized, washed twice with PBS buffer (pH 7.4) and 25 µl of the cell suspension was stained with Hoechst 33258 for 10 min at room temperature in the dark. The condensed or fragmented nuclei of apoptotic cells were

observed using above fluorescence microscopy with DAPI filter (excitation [Ex], 365 nm and emission [Em], 480 nm).

2.3.4. DNA fragmentation

Cells were collected after 24 h of treatment with NPs at the mentioned concentrations. DNA was extracted according to the standard protocol for DNA isolation.[17] Briefly, cells were treated with different concentrations of NPs for 24h, cells were harvested, counted and washed with PBS at 4°C. The cells were pelleted by centrifugation at 200 g at 4°C. The pellet was suspended in DNA lysis buffer [1M Tris (pH 8.0), 0.5M EDTA and 75% sodium lauryl sarcosine] and incubated overnight with proteinase K (0.5 mg/ml) at 50°C. After overnight incubation RNase was added and incubated for an hour at 50°C. DNA was extracted using phenol: chloroform (1:1 v/v) and then electrophoresed in 2% agarose gel for 2 h at 50V. The gel was stained with EB (0.5 µg/ml) followed by UV exposure and photographed in Gel Doc XR+ (Bio-Rad, Hercules, CA, USA).

2.3.5. Determination of intracellular ROS

Cellular oxidative damage induced by AgNPs was quantified using cell permeable dye carboxy-H2DCFDA (Invitrogen). This compound is oxidized by ROS into fluorescent carboxydichlorofluorescein (DCF) inside the cells. Briefly, experimental cells were incubated with 10 µM DCFHDA for 30 min at 37°C in the dark, washed twice with PBS and fluorescence resulting from oxidation of dye in the cells were measured with an excitation wavelength of 480nm and an emission wavelength of 530 nm.

2.3.6. Semi –quantitative RT-PCR and quantitative real time PCR analysis

Total RNA was extracted from experimental cells using Trizol reagent (Invitrogen, USA). RNA isolated from cells was reverse-transcribed and amplified using the one-step RT– PCR System (Fermentas, USA). Forward and reverse primers for Bax (NM_001188.3) were 5'- GCC ACC AGC CTG TTT GAG -3' and 5'-CTG CCA CCC AGC CAC CC-3', for Bcl2 (NM_000657.2) were 5′-TAT AAG CTG TCG CAG AGG GGC TA-3′ and 5′- GTA CTC AGT CAT CCA CAG GGC GAT-3′and for GAPDH (NM_002046.3) were 5′- AAT CCC ATC ACC ATC TTC CA -3′ and 5′- CCT GCT TCA CCA CCT TCT TG-3′, respectively. PCR condition was set as follows: 94°C for 5 min; 35 cycles of 94°C for 1 min, 55–62°C for 1 min, 72°C for 1 min and final extension step of 72°C for 10 min. The products were verified by agarose gel electrophoresis as well. The level of GAPDH gene expression served as an internal control. From above RNA cDNA was prepared by using Qiagen cDNA preparation kit. The mRNA expression of p53 was detected after NPs treatment by using p53 forward and reverse primers as 5'-AATCATCCATTGCTTGGGACG-3'; 5'-CCGCAGTCAGATCCTAGCG -3' in 7500 real-time PCR System (Applied Biosystems) with the SYBR green Master mix (Invitrogen). Relative p53 mRNA levels were determined by comparing the PCR cycle thresholds between cDNA of a specific gene and histone (ΔCt).

2.3.7. Western blotting

MCF-7 cells were cultured in 6-well plates and then treated with or without NPs for 24 h. The cells were then lysed in the buffer containing 50 mM Tris–Cl (pH 8.0), 150 mM NaCl, 0.02% sodium azide, phenylmethane sulfonyl fluoride (PMSF), aprotinin, and 1% Triton X100, and centrifuged at 12,000 rpm for 30 min at 4°C. Quantified proteins were electrophoresed in SDS-PAGE. The separated proteins were transferred to nitrocellulose membranes. Membranes were washed with tris-buffered saline Tween-20 (TBST), blocked with 5% skimmed milk for 1 h at 37°C, incubated overnight at 4°C with either goat anti-rabbit caspase 3, 8 and 9 or b-actin antibodies at the manufacturer recommended dilutions. After incubation, the membrane washed with TBST buffer. The membranes were then incubated with secondary mouse anti-goat peroxidase conjugated antibodies (Cell Signalling technologies, USA) for 1 h at 37°C. After washing membranes with TBST, they were developed with DAB chromogenic detection method and scanned.

2.3.8. Analysis of Cell cycle disruption by Flow Cytometry

After NPs exposure, cells (1 x106 in 10ml) were trypsinized and fixed in ethanol and stored at 4°C until assayed. Samples were pelleted at 2,000 rpm for 5 minutes, pellets were washed twice with ice-cold PBS and centrifuged further for 5 minutes. Subsequently, pellets were resuspended in 0.5 ml DNA staining solution (25 µg/ml propidium iodide, 100 µg/ml RNase A in PBS) and incubated at 37°C for 30 minutes in the dark. Cell cycle analysis (10,000 events for each sample) was performed using FACS Calibur flow cytometer with CELL Quest software (BD Biosciences, San Jose, CA, USA) and expressed as fractions of cells in different cell cycle phases. Samples were run in triplicate and each experiment was repeated three times.

3. Results and Discussion

The uses of existing drugs for cancer chemotherapy were limited with poor specificity, high cost, high toxicity, side effects and emergence of drug resistance. To overcome this situation nano sized materials were intensively studied because of its unique physiochemical properties, stability and biological fate.[18-19] In particular, biogenesis of nanomaterials was found as viable and facile alternative strategy due to its green chemistry approach. Apart from its eco-friendly scheme, interaction of biocompounds with noble metals offers multifunctional hybrid nanomaterials for cancer diagnosis and therapy.[20-21] Our study was executed in view to reveal the molecular mechanism involved in biogenic NPs induced cytotoxicity against human breast carcinoma cells. Cell viability assay clearly explains the cellular response to biogenic metal NPs, especially size, morphology and surface functionalization have shown major influence on biokinetics and toxicity.[22]

3.1 Synthesis and charecterization of biogenic NPs

As reported in our previous studies[13-14], synthesized Ag and AuNPs using the leaf extract of *P.hexandrum* was initially confirmed with the development of yellowish brown and ruby red colour respectively due to the exicitation of surface plasmonic vibrations. UV-Visible spectroscopy of synthesized AgNPs produces an absorbance spectrum at 420nm whereas AuNPs have shown SPR peak at 530nm. TEM micrographs of syntehsized Ag and AuNPs have shown stable, crystalline and polydisepersed with the size range of 12-40 nm and 5-35 nm correspondingly. We also noticed a thin-layer of biomolecule coating on the surface of the nanoparticles which prevents the aggregation of NPs. Interestingly, XRD diffractogram of synthesized NPs gives bragg's reflections at (1 1 1), (2 0 0), (2 2 0) and (3 1 1) which strongly evidenced that synthesized NPs were face centred cubic (Fcc) crystalline in nature. Further, FTIR analysis revealed that the water soluble phenolic constituents of *P.hexandrum* mainly involves in the reduction and stabilization of nanoparticles. Moreover, the transmittance has clearly exposed the interaction of phenolic compounds with O–H functional groups may accomplish reduction process.

3.2. Assay for cell viability

MTT data clearly reveals that treatment of NPs decreased the MCF-7 cell viability partially in dose and time dependent manner. From the Fig.1 it is evident that 100% cell mortality rate was noticed at the maximum concentration after 48 h. Consequently, 50% (IC50) inhibitory concentration of Ag and AuNPs were fixed to be 100µl/ml (Fig. 1a) and 200µl/ml (Fig. 2b) respectively. As described previously by various investigators, the toxicity of AgNPs could be based on their surface morphology and size.[23] In a recent study, it was noticed that biogenic AgNPs synthesized using the leaf extract of *D.falcata* with the size range of 5–45 nm has shown enhanced cytotoxicity against human breast carcinoma cells (MCF-7) compared to aqueous plant extract.[24] Likewise gold NPs also displayed size dependent cytotoxicity in treated fibroblasts, epithelial cells and melanoma cells.[25] Another report also showed that gold nanoparticles induce cytotoxicity against human breast epithelial (MCF-7) cells in a dose dependent manner at the concentration range between 25-200 µg/mL.[26]

3.3. Measurement cytomorphological changes in MCF-7

Phase contrast microscopy demonstrated dose dependent detachment of nonviable cells from the surface of culture plates (Fig.2). MCF-7 cells exposed to NPs showed morphological changes including cell shrinkage and formation of apoptotic bodies. This result was highly corroborate with an earlier study where synthesized AgNPs from the leaf extract of *Vitex negundo* L. induce cellular shrinkage in treated human colon cancer cell line (HCT15).[27] These morphological changes are due to the activation of caspase cascades, which cleaves the specific substrates responsible for the DNA repair activation. When NPs come in contact with the cells they were taken up by a variety of mechanisms like clathrin-dependent endocytosis and macropinocytosis.[28-29] These can lead to activation of cellular signalling processes producing reactive oxygen species (ROS), inflammation and finally cell cycle arrest or cell death.[30]

3.4. Detection of NPs induced apoptosis in MCF-7 cells

Apoptosis is the key event in cancer therapy that can be measured with the activation caspase-cascade, chromatin aggregation, partition of the cytoplasm and nucleus into membrane-bound vesicles (apoptotic bodies) that contain ribosomes, morphologically intact mitochondria, and nuclear material.[31] In this study NPs treated MCF-7 cells loses their viability in a time and dose dependent manner. The ability of NPs (Ag and AuNPs) to induce apoptosis was determined by AO-EB staining. After treatment with mentioned concentration, the cells were harvested and stained with AO-EB as mentioned in the materials and methods section. Cells exposed to NPs showed greater apoptotic effect (Fig 3a) when compared to control cells. Similar phenomenon was reported with *A. calamus* rhizome extract AgNPs that activates apoptosis in treated HeLa cells.[32] Furthermore, the effects of NPs on MCF-7 cells gross nuclear morphology were observed under fluorescence microscopy after Hoechst 33258 staining. After the treatment with different concentration of NPs for 24 h, MCF-7 cells began to exhibit apoptotic characteristics such as nuclear blebbing, nuclear condensation and fragmentation. In the control group, the cells were regular in morphology and grew fully in patches and were confluent, rarely sloughing off (Fig.3b). Interestingly, Fig. 3c shows the percentage distribution of apoptotic cells (viable, early, late and necrotic cells).

3.5. Effect of NPs induced DNA damage on MCF-7 cells

NPs have induced apoptosis in treated MCF-7 cells through DNA damage that have been confirmed with DNA fragmentation assay. The induction of DNA single strand break is often used to predict oxidative damage of tumour cells. As shown in (Fig. 3d) NPs pre-treatment at the concentration (Ag-200µl) and (Au-200 & 400 µl) respectively cause the formation of DNA ladder which depicts that NPs has induced cell death through apoptotic pathway. However, at minimal dosange of AgNPs (100 µl) does not cause the formation of DNA laddering. It is now well established that excessive generation of ROS triggers signal transduction pathways leading to apoptosis.[29-30] In reliable with several studies our data clearly proved that NPs induced cytotoxicity was initially triggered by oxidative stress mediated DNA damage. An important aspect of DNA damage is the formation free radicals that mainly cause single strand break. The DNA laddering was observed in the present study reveals that generation of ROS favours over DNA damage leading to cell death. An earlier study proved that highly reactive hydroxyl radicals released by the AgNPs attack cellular components including DNA, lipids, and proteins that cause various kinds of oxidative damages.[31]

3.6. NPs induce apoptosis via mitochondria- and caspase-dependent pathway

To study the possible molecular mechanisms of NPs-mediated cell death, the apoptotic regulators have been measured through mRNA and protein expression patterns. In order to confirm NPs induced ROS mediated the apoptotic pathway, the mRNA levels of Bcl- 2 and Bax were semi-quantitatively determined through RT-PCR. Interestingly, after the NPs treatment level of Bax and GAPDH were upregulated whereas the level of Bcl-2 was found to be decreased in dose dependent manner (Fig. 5a). However, the activation of mitochondrial apoptotic pathway in caspase- 6 and caspase- 9 showed a significant increase after 24 h of treatment with NPs (Fig. 5b). Increase in the synthesis level of the poly (ADP-ribose) polymer (PARP) depicts that NPs induce apoptotic and necrotic cell death was mediated via Bcl-2/Bax proteins and caspase cascade. All the expression was normalized with the levels of the β-actin expression. These results clearly indicate that the mitochondrial signalling pathway was playing a crucial role in NPs-induced apoptosis in MCF-7cells. According to the present study NPs trigger apoptotic protein Bax and down regulates Bcl-2 of which results in activation of programmed cell death. It is well known that anti-apoptotic members of the Bcl-2 family specifically inhibit the release of certain apoptogenic factors.[32] Down-regulation of Bcl-2 is very crucial in caspase activation and the induction of apoptosis because it releases cytochrome C from mitochondria.[6] However, Bcl-2 heterodimerization with Bax, when the Bcl-2 expression level is down regulated there was up regulation of Bax expression, homodimers of Bax will always be formed and apoptosis will be stimulated. Earlier studies have proved that the ratio between pro- and anti-apoptotic proteins determine the susceptibility of cells to a death signal.[33] Besides, caspases-cascade (cysteine-requiring aspartate proteases) was the most important characteristic of apoptosis, which can be triggered by several groups of so called initiators (e.g., caspases- 8, -9) and effectors (e.g., caspases-3, -7, -6). Among this caspase-3 and 6 plays a crucial role in apoptosis, whose activation is mediated by inhibitor caspases such as caspase-8 and 9. Several studies pointed out that the activation of caspases has shown direct effect on mitochondrial membrane potential.[34-35] However, further investigations are required to elucidate the potential cytotoxicity of different cell lines to NPs in *vitro* as well as to assess the biocompatibility and biosafety of such particles *in vivo* based on their size.

3.7. Cell cycle arrest

Generally, apoptosis and the cell cycle arrest are closely related.[36] In our study NPs treated MCF-7 cells proportion was found decreased in the G1 and increased in subG1, phases of cell cycle (Fig. 6). Furthermore as shown in Fig.7, mRNA levels of p53 in NPs treated cells was upregulated which confirms the p53 induced DNA damage. These data clearly authorizes that developed metal nanoformulations actively inhibits the progression of MCF-7 cell cycle at G1 phase and accumulation of cells and subG1 confirms the activation of apoptotic pathway after NPs exposure.

.

4. Conclusion

To summarize the present study, biogenic metal NPs shows prominent anticancer activity against MCF-7 cells. At minimal dosage NPs triggers mitochondrial-driven apoptosis via activation of procaspase-3 and -9. In addition, decreased expression of Bcl-2, increased expression of Bax and cleaved PARP authorizes the enhanced anticancer activity of bionanoparticles. The overall results suggested that biogenic metal nanoformulations can be potentially developed into cost-effective, commercially viable drug candidature to combat breast cancer. In future, the synthesized NPs have to be assessed against different types of cancer cells. Moreover, it is very important to assess the preclinical insights and other molecular signalling pathways including angiogenesis need to be investigated and these studies are in progress.

Author address
[a]National Centre for Nanosciences and Nanotechnology, University of Madras, Guindy campus, Chennai 600025, India. Email: jeymuruga@gmail.com
[b]Laboratory[1] of Molecular Oncology Clinic and Policlinic for Oncology University Hospital Zurich Häldeliweg 4, 8044 Zurich
[c]Department of Biotechnology and Genetic Engineering,
[d]Department of Biomedical Sciences, Bharathidasan University, Tiruchirappalli 620024, India
$ Authors contributed equally

Reference

1 F.Brayand, B.Moller, Nat. Rev. Cancer, 2006, **6**, 63.
2 D.M. Parkin, F.Bray, J. Ferlay, P.Pisani, CA Cancer J Clin., 2005, **5**, 574.
3 A.S.Narang, D.S.Desai, Pharmaceutical Perspectives of Cancer Therapeutics, 2009, 49.
4 P.Parhi, C.Mohanty, S.K.Sahoo, Drug Discovery Today, 2012, **17**, 1044.
5 R.Misra, S.Acharya, S.K.Sahoo, Drug Discovery Today, 2010, **15**, 842.
6 C.Chang, Y.Q.Zhu, J.J.Mei, S.Q.Liu, J.Luo, J Exp.&Cli. Cancer Res., 2010, **29**, 1
7 J.M.Adams, S.Cory, Oncogene, 2007, **26**, 1324.
8 S.Cory, D.C.Huang, J.M.Adams, Oncogene, 2003, **22**, 8590.
9 A.R.Gliga, S.Skoglund, I.O.Wallinder, B.Fadeel, H.L.Karlsson, Particle and Fibre Toxicology, 2014, **11**, 1.
10 Y.Zhang, D.Xu, W.Li, J.Yu, Y.Chen, Journal of Nanomaterials, 2012, 1.
11 T.H.Kim, M.Kim, H.S.Park, U.S.Shin, M.S.Gong, H.W.Kim, Journal of biomedical materials research A, 2012, **100**, 1033.
12 P.V. AshaRani, G.L.K. Mun, M.P. Hande, S.Valiyaveettil, ACS Nano, 2009, **3**, 279.
13 M. Jeyaraj, M. Rajesh, R. Arun, D. MubarakAli, G. Sathishkumar, G. Sivanandhan, G. KapilDev, M. Manickavasagam, K. Premkumar, N. Thajuddin, A. Ganapathi, Colloids Surf. B: Biointerfaces, 2013, **102**, 708.
14 M.Jeyaraj, R.Arun, G.Sathishkumar, D.MubarakAli, M.Rajesh, G.Sivanandhan, G.Kapildev, M.Manickavasagam, N.Thajuddin, A.Ganapathi, Materials Research Bulletin, 2014, **52**, 15.
15 T.Moshmann, J.Immunol. Method 1983, **65**, 55.

16 A.Gorman, J.McCarthy, D.Finucane, W.Reville, T.G. Cotter, S.J. Martin and T.G. Cotter, eds. London: Portland Press Ltd., 1996, pp. 1–2.
17 R.T.Allen, W.J.Hunter, D.K.Agrawal, J. Pharmacol.Toxicol. Methods, 1997, **37**, 215.
18 S.C.Boca, M.Potara, A.M.Gabudean, A.Juhem, P.L.Baldeck, S.Astilean, Cancer Lett. 2011, **311**, 131.
19 H.K.Chan, Adv. Drug Deliv. Rev., 2011, **63**, 405.
20 S.Gurunathan, J.Raman, S.N. Malek, P.A.John, S.Vikineswary, Int. J. Nanomedicine, 2013, **8**, 4399.
21 A.Nel, T.Xia, L.Madler, N.Li, Science, 2006, **311**, 622.
22 M.I.Sriram, K.Kalishwaralal, S.Barathmanikanth, S.Gurunathan, Nanoscience Methods, 2012, **1**, 56.
23 G.Sathishkumar, C.Gobinath, A.Wilson, S.Sivaramakrishnan, Spectrochimica Acta Part A: Molecular and Biomolecular Spectroscopy, 2014, **128**, 285.
24 Y.Pan, S.Neus, A.Leifert, M.Fischler, F.Wen, U.Simon, G.Schmid, W.Brandau, W.J.Dechent, Small, 2007, **3**, 1941.
25 M.E.Selim, A.A.Hendi, Asian Pacific Journal of Cancer Prevention 2012, **13**, 1617.
26 C. Greulich, J. Diendorf, T. Simon, G. Eggeler, M. Epple, M. Köller, ActaBiomater., 2011, **7**, 347.
27 M.Ahamed, M.A.Siddiqui, M.J.Akhtar, I.Ahmad, A.B.Pant, A. HA, Biochem.Biophy.Res., 2010, **396**, 578.
28 M.Ott, V.Gogvadze, S.Orrenius, B.Zhivotovsky, Apoptosis, 2007, **12**, 913.
29 S.Ueda, H.Masutani, H.Nakamura, T.Tanaka, M.Ueno, J.Yodoi, Antioxid Redox Signal, 2002, **4**, 405.
30 M.J.Piao, K.A.Kang, I.K.Lee, H.S.Kim, S.Kim, J.Y.Choi, J.Choi, J.W.Hyun. Toxicol Lett., 2011, **201**, 92.
31 N.Xiang, R.Zhao, W.Zhong, Cancer Chemother Pharmacol., 2009, **63**, 351.
32 S.Cory, J.M.Adams, Nat. Rev. Cancer, 2002, **2**,647.
33 D.X.Hou, Curr Mol Med., 2003, **3**, 149.
34 S.R.Samarakoon, I.Thabrew, P.B.Galhena, K.H.Tennekoon, Tropical Journal of Pharmaceutical Research, 2012, **11**, 51.
35 A.B.G.Serrano, M.A.Martı´n, L.Bravo, L.Goya, S.Ramos, The Journal of Nutrition Biochemical, Molecular, and Genetic Mechanisms, 2006, 2715.

Figure 1

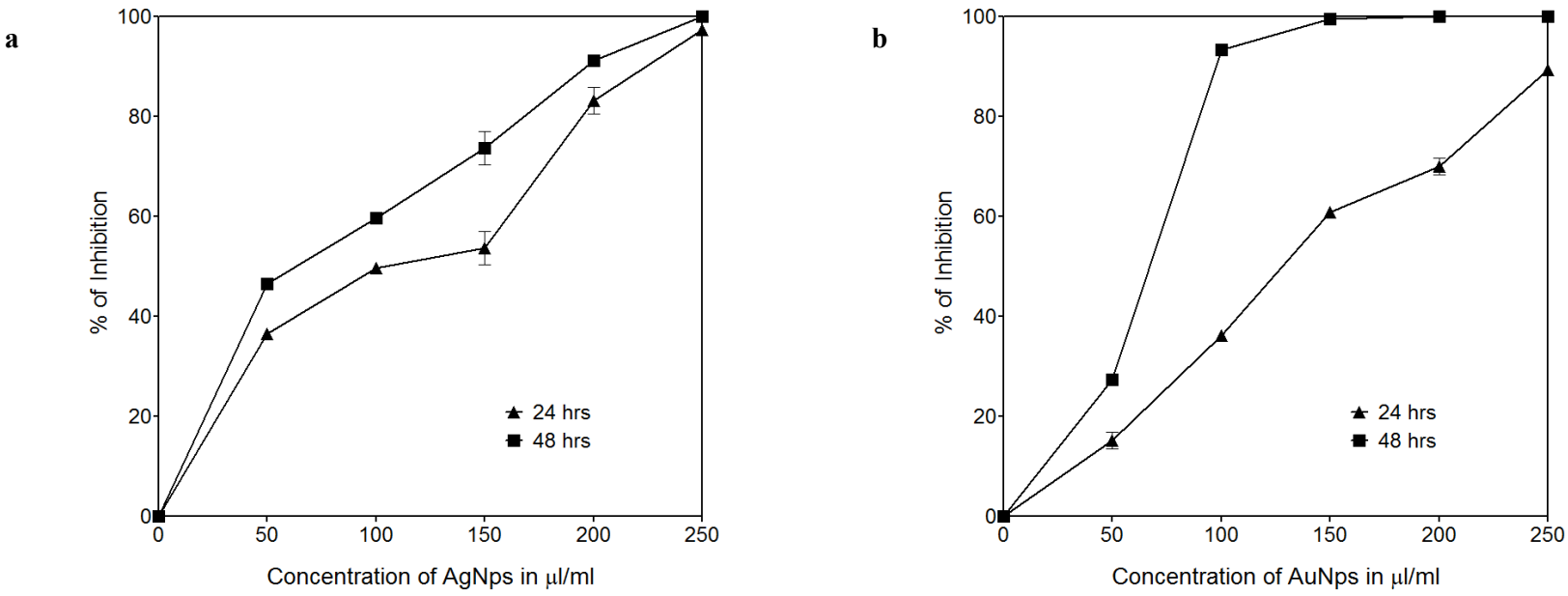

Fig.1. Inhibitory effects of the biosynthesized Au and AgNPs on MCF-7 cells treated with different doses (50, 100, 150, 200 and 250µl/ml) for 24 and 48h. All the data is expressed as the mean ± SD of the three experiments with duplicate wells.

Figure 2

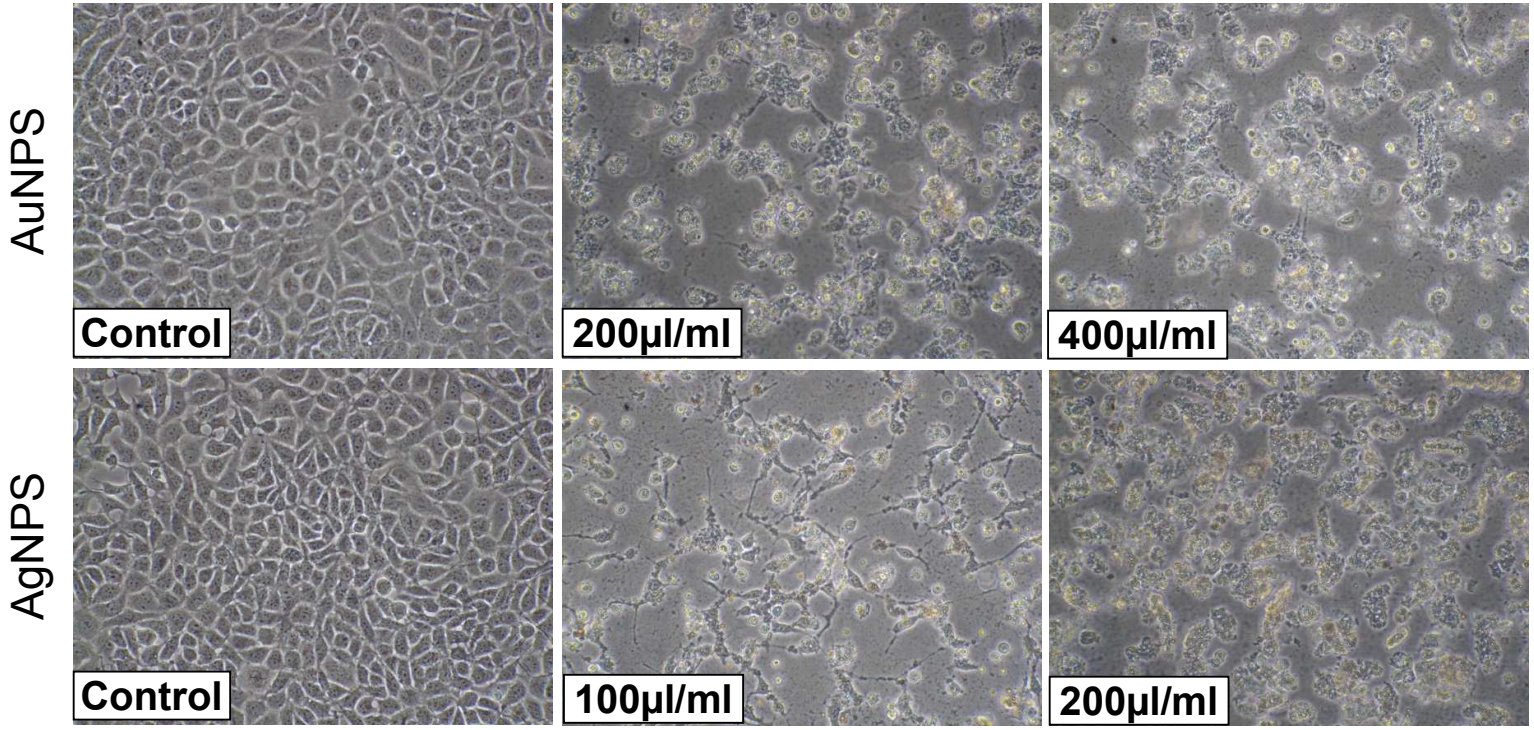

Fig.2 Morphological characterization under phase contrast microscopy of cell death induced by the Au and AgNPs in MCF-7 cells for 24 hours. Magnification at 200x.

Figure 3

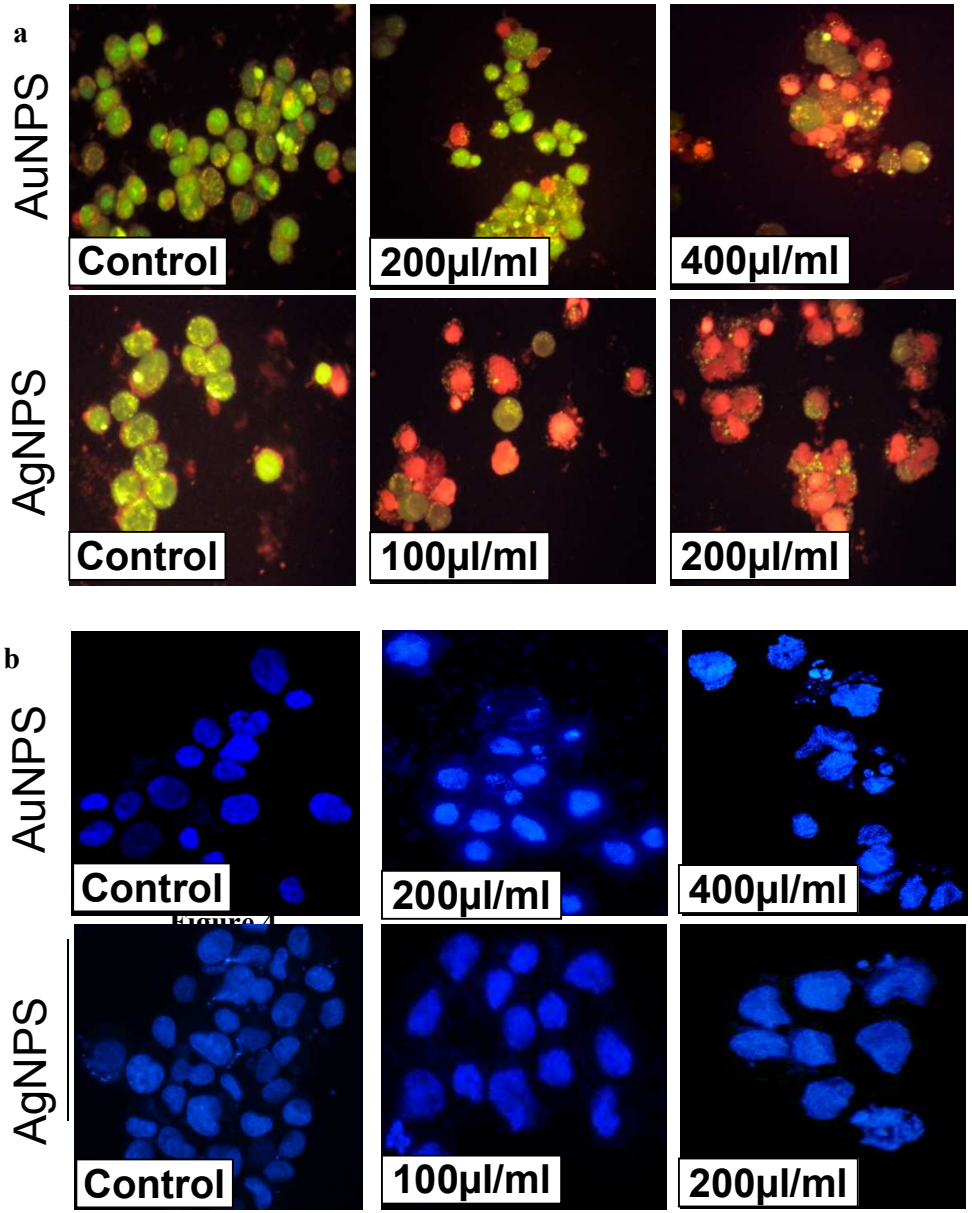

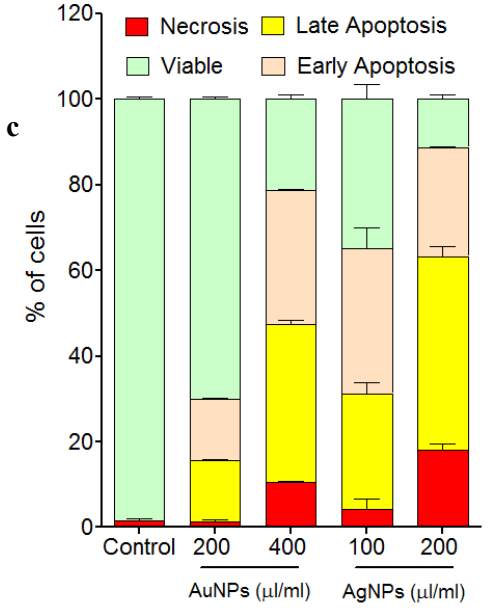

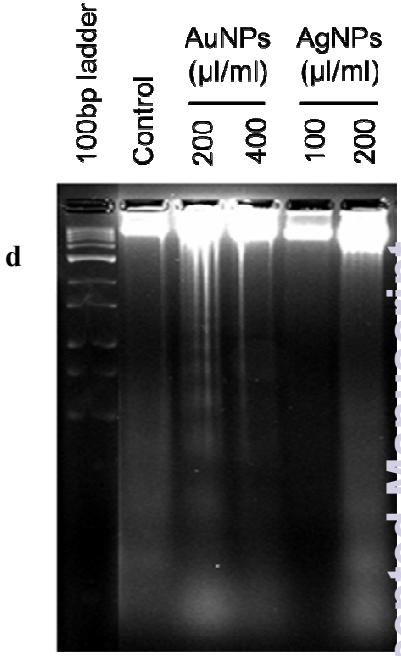

Fig. 3. Au and AgNPs induced apoptosis in MCF-7 cells. **A.** Photomicrographs of AO/EB stained MCF-7 cells incubated for 24 h with either Au or AgNPs. Viable (light green), early apoptotic (bright green fluorescing), late apoptosis (red to orange fluorescing) and necrosis (red fluorescing) cells were observed. **B.** Representative fluorescent micrographs of MCF-7 cells stained with Hoechst 33258 fluorescent dye after 24 h incubation with either Au or AgNPs. Magnification at 200x. **C.** Percentage distribution of apoptotic cells (viable, early, late and necrotic cells). **D.** AgNPs induced inter nucleosomal DNA fragmentation. MCF-7 cells were treated with 0, 100 and 200µl/ml of AgNPs for 24 h. Cells were harvested and DNA was extracted as described in the Materials and Methods section. Fragmented DNA was analyzed by agarose gel electrophoresis. Representative gels from one of the three experiments.

Figure 4

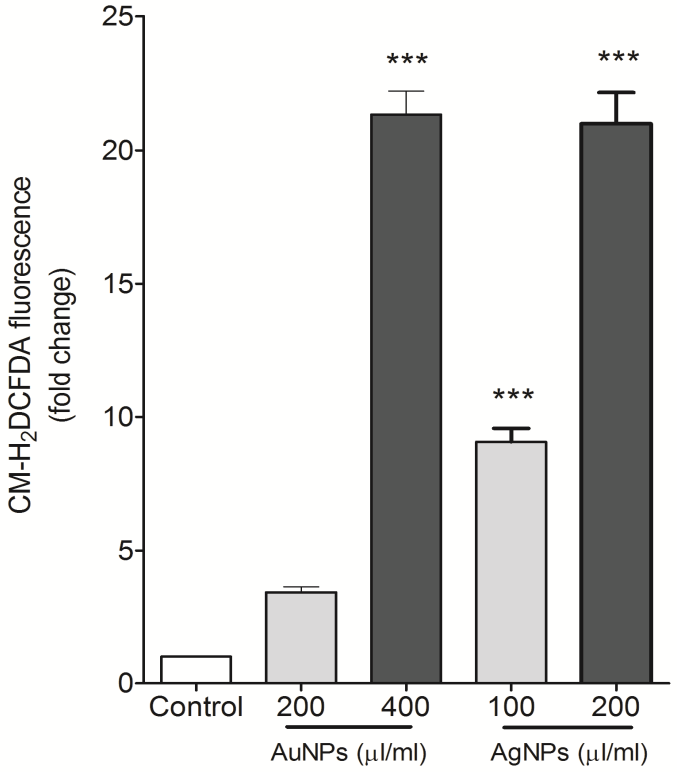

Fig. 4. Au and AgNPs induced ROS in MCF-7 cells. MCF-7 cells were treated with different concentration of Au or AgNPs for 24 h and ROS was determined as mentioned in the Materials and Methods section. All the data is expressed as the mean ± SD of the three experiments with duplicate wells. Statistically significant difference as compared to the controls (* $p<0.05$ for each).

Figure 5

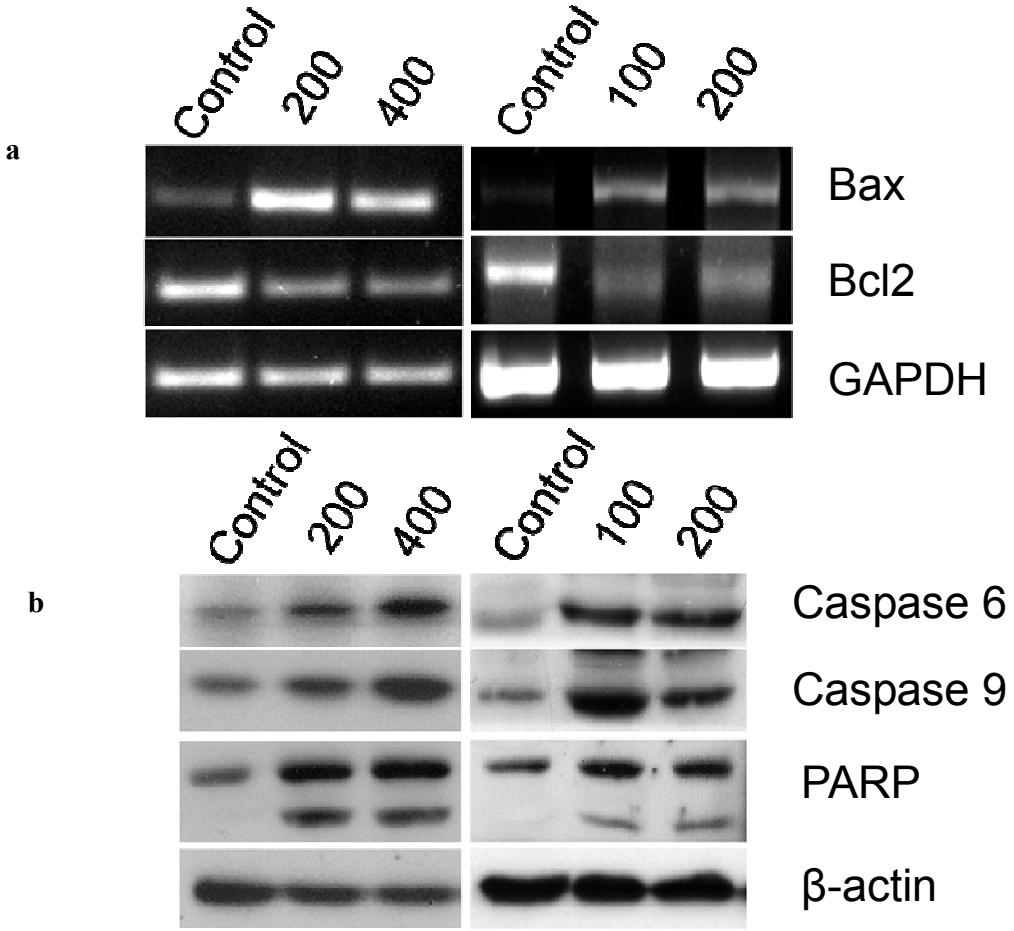

Fig. 5. A. Effect of Au or AgNPs on mRNA levels of Bcl_2 and Bax in MCF-7 cells. **B.** Effect of AgNPs on Caspase 6, 9 and PARP protein expression as determined by Western blot analysis in MCF-7 cell line. β-actin was used as the control. Representative Western blots of experiments performed in triplicates.

Figure 6

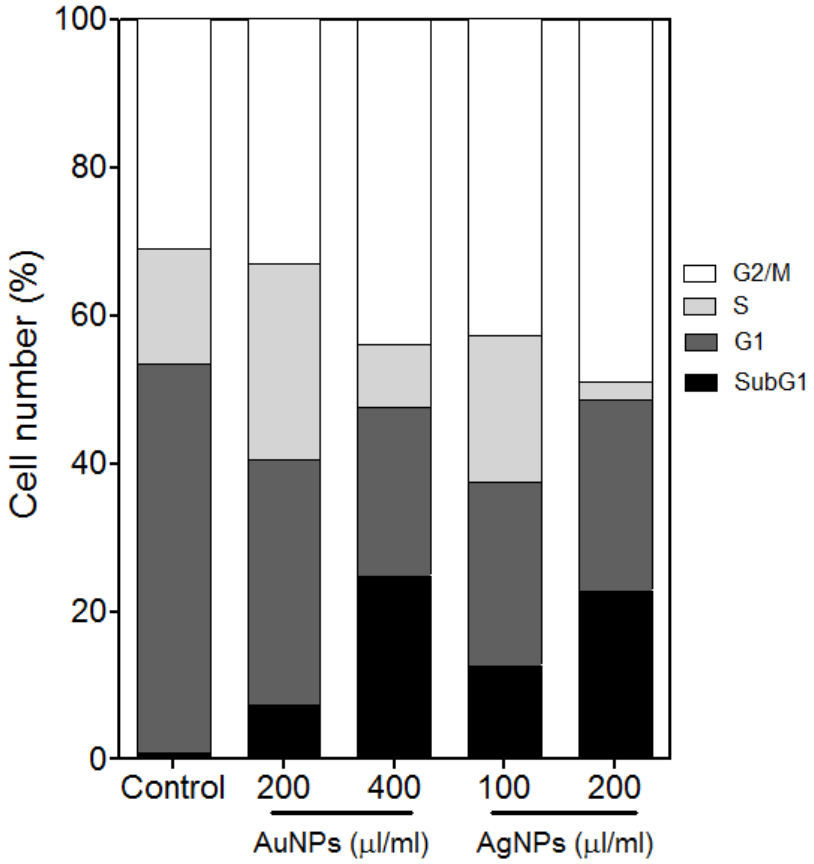

Fig. 6. Effect of Au or AgNPs on cell cycle distribution of MCF-7 cells. All the data is expressed as the mean ± SD of the three experiments.

Figure 7

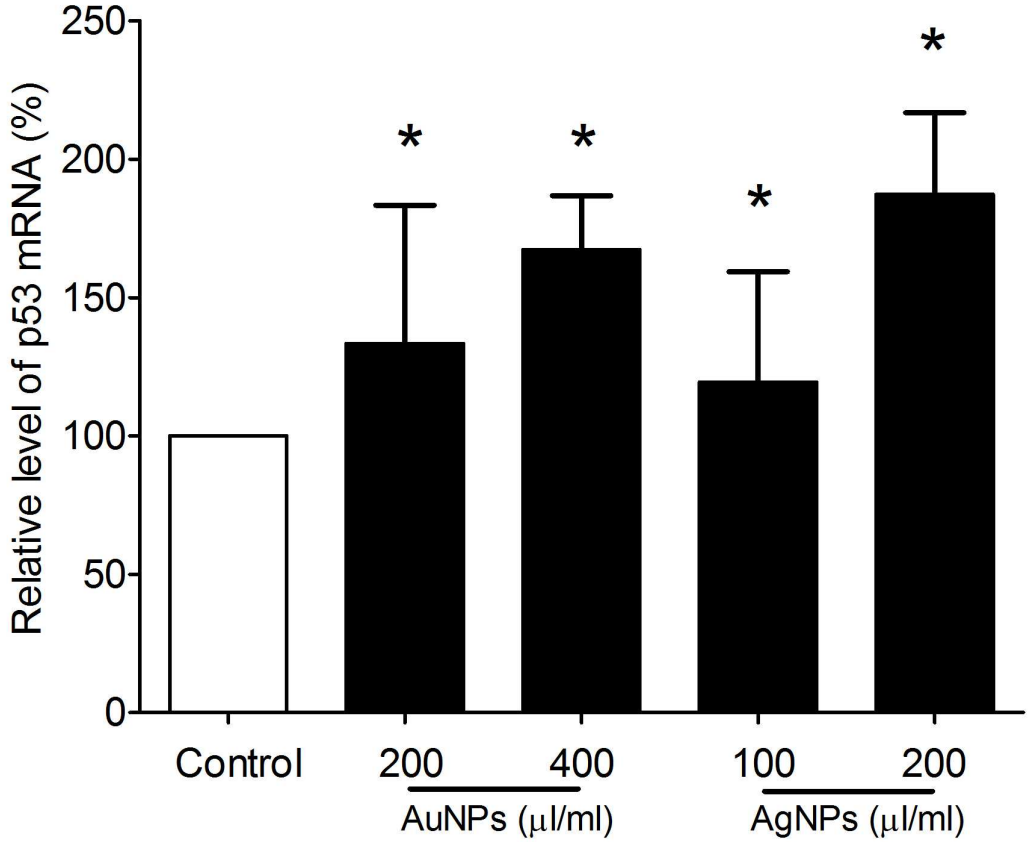

Fig.7. Quantitative real-time PCR analysis of p53 mRNA levels in MCF-7 cells exposed to Au & Ag NPs. Data represented are mean ± SD of three identical experiments made in three replicate. Statistically significant difference as compared to the controls (* $p<0.05$ for each).